



## Preparation of activated carbon from *Camellia oleifera* shell and its application to adsorption of hexavalent chromium from aqueous solution: kinetics, equilibrium, and thermodynamics

Zhigong Zheng<sup>a,\*</sup>, Haoyue Zhao<sup>a</sup>, Xuehui Lin<sup>a</sup>, Jinbei Yang<sup>b,\*</sup>, Ronghui Shi<sup>a</sup>

<sup>a</sup>College of Ecological Environment and Urban Construction, Fujian University of Technology, Fuzhou 350108, Fujian, China, Tel. +86-18396533563; emails: zhigongzheng@fjut.edu.cn (Z. Zheng), 1123208378@qq.com (H. Zhao), 1510435069@qq.com (X. Lin), shironghui@fjut.edu.cn (R. Shi)

<sup>b</sup>School of Ocean Science and Biochemistry Engineering, Fuqing Branch of Fujian Normal University, Fuzhou 350300, Fujian, China, Tel. +86-15280192415; email: yangjinbei@sina.com (J. Yang)

Received 11 December 2019; Accepted 18 April 2020

### ABSTRACT

Preparation of the adsorbent was performed by pyrolysis carbonization and followed by potassium hydroxide (KOH) activation of *Camellia oleifera* shell under the nitrogen atmosphere. Through the thermogravimetric-derivative thermogravimetric analysis, the range of carbonization temperature was set from 300°C to 400°C increased 50°C at a time. The optimum carbonization and activation conditions were investigated by the orthogonal experiment. The activated carbon was characterized by scanning electron microscopy, Brunauer–Emmett–Teller, and Fourier transform infrared spectroscopy. The adsorption of hexavalent chromium (Cr(VI)) from aqueous solution by *C. oleifera* shell activated carbon was carried out with batch adsorption experiments. The effects of initial pH value, adsorbent dosage, the temperature on the adsorption were studied. The results indicate that the activated carbon is an effective adsorbent with a high surface area (1,585.60 m<sup>2</sup>/g) and a large pore volume (1.055 cm<sup>3</sup>/g). The adsorption process follows the pseudo-second-order kinetic model. The adsorption equilibrium data obtained at 25°C, 35°C, and 45°C fit better with the Freundlich model than Langmuir model and the thermodynamics parameters,  $\Delta H^\circ$ ,  $\Delta S^\circ$ , and  $\Delta G^\circ$  were calculated. It indicates that the process of Cr(VI) adsorption on activated carbon is entropy-driven and endothermic. The results illuminate that *C. oleifera* shell activated carbon is an effective adsorbent for adsorbing Cr(VI) from aqueous solutions.

**Keywords:** Hexavalent chromium; Adsorption; Isotherm; Kinetics; *Camellia oleifera* shell

### 1. Introduction

Heavy metals in wastewater are a truly big environmental pollution problem due to the properties of their non-degradability and accumulation in organisms [1]. Hexavalent chromium (Cr(VI)) ion, one kind of the heavy metals, is widely detected in wastewater discharged from various industrial processes, for instance, electroplating industries, oil refining, and metallurgy industry [2,3]. Cr(VI)

is widely known to be poisonous to most life in the earth, even at low concentrations [4].

There are many methods for the treatment of wastewater with Cr(VI), such as photocatalytic reduction [5,6], electrochemical reduction [7], membrane filtration [8], and adsorption [9,10]. Among them, physical adsorption is the common method to remove Cr(VI) in the wastewater due to its easy operation, high-efficiency, and inexpensive [11].

\* Corresponding authors.

Various kinds of adsorbents have been studied on the removal of Cr(VI), such as mesoporous silica [12,13], cellulose [14], graphene [15], polymeric adsorbent [16], activated carbon [17], etc.

Activated carbon is known as one kind of effective adsorbent because of its high specific surface area and large pore volume. It is confirmed that many agricultural waste materials can be used to prepare activated carbon, such as tea leaf [18], cotton processing wastes [19], sawdust [20], the residue of rice husk [21], cow manure [22], grape bagasse [23], *Camellia oleifera* shell [24], etc. *C. oleifera* shell is a typical agricultural waste material among camellia oil production and is an appropriate raw material to prepare activated carbon [25].

Thermogravimetric analysis (TG) has long been used to study the thermal behavior of organic matters. Carbonization is an important step of the preparation of activated carbon. Through the pyrolysis of raw materials, carbide with initial pores and certain mechanical strength can be obtained, which was conducive for activation.

In this study, TG analysis was applied to confirm the temperature range of the carbonization. The activated carbon was synthesized by *C. oleifera* shell and characterized by scanning electron microscopy (SEM), Brunauer–Emmett–Teller (BET), and Fourier transform infrared spectroscopy (FT-IR). The efficiency of activated carbon on the adsorption removal of Cr(VI) ions from aqueous solutions was also evaluated. Preparation of the adsorbent was performed by pyrolysis carbonization and followed by KOH activation of *C. oleifera* shell under the nitrogen atmosphere [2]. Solution pH, adsorbent dosage, absorption temperature, and contact time, were studied to investigate their effects on the process of Cr(VI) adsorption in the aqueous system. Moreover, kinetics and isotherms of Cr(VI) adsorption were also investigated.

## 2. Experimental

### 2.1. Materials

*C. oleifera* shell were obtained from Ganzhou in China, which were dried in sunshine;  $K_2Cr_2O_7$  ( $\geq 99.8\%$ ), 1,5-diphenyl-carbazide, potassium hydroxide, potassium bromide, and sulfuric acid were purchased by Sinopharm Chemical Reagent Co., Ltd., (Shanghai, China), with all chemicals of analytical grade or above and used as received. Deionized water was obtained using a Millipore Milli-Q ultrapure water system (Bedford, MA, USA).

### 2.2. Analysis method

The concentrations of Cr(VI) ions were measured by the colorimetric technique coupled to UV-Vis spectroscopy (Model 7200, Shanghai Unico Instrument Co., Ltd., Shanghai, China) at 540 nm. The standard curve of Cr(VI) concentration ( $y$ , mg/L) to absorbance ( $x$ ) was obtained as follows:  $y = 1.4160x + 0.0057$ , the scope of  $x$  is 0–0.7, and the determination coefficients of the curves was 0.9994.

### 2.3. Preparation of activated carbon adsorbents

The *C. oleifera* shell were adequately cleaned in distilled water and dried at 105°C for 10 h by an electric thermostat blast dryer (model DHG 9076A, Shanghai Jinghong Laboratory Instrument Co., Ltd., Shanghai, China). After that, they were crushed by a high-speed multifunction grinder (model DS-T250, Shanghai Dingshuai Instrument Co., Ltd., Shanghai, China) and separated to the size of 100 mesh with sieves. A mass of 100 g of the powder was carbonized under  $N_2$  atmosphere at 300°C–400°C for 1 h in a box-type resistance furnace (model SX2-4-10, Shanghai Experiment Instrument Co., Ltd., Shanghai, China). Then the char produced from the carbonization process was mixed with potassium hydroxide (KOH) with a 1:(1–3) (w/w) ratio. The mixture was then activated under  $N_2$  atmosphere at 600°C–800°C for 0.5–1.5 h. They were cooled, then washed with distilled water to neutral, and dried at 100°C for 24 h. Then, the *C. oleifera* shell activated carbon was obtained and stored in desiccators for use in adsorption studies.

In order to optimize the preparation process of *C. oleifera* shell activated carbon, an orthogonal experimental design  $L_9(3^4)$  was used as listed in Table 1. The mass ratio of KOH to carbonized material, activation time, activation temperature, and carbonization temperature were set as four influencing factors. The values of each parameter were chosen as follows in Table 1. The equilibrium adsorption capacity of Cr(VI) on *C. oleifera* shell activated carbon were set as the test index of the orthogonal experiment.

### 2.4. Characterization

Thermo-gravimetric analysis of the powder crushed by *C. oleifera* shell (raw powder) was performed by thermal gravimetric analyzer (NETZSCH TG 209 F3 Nevio, Germany). Surface morphology of the activated carbon prepared from *C. oleifera* shell was studied by scanning electron microscope (Hitachi S-4800, Japan) in order to make

Table 1  
Orthogonal experimental design  $L_9(3^4)$  on the preparation of activated carbon

Factor levels	A (carbonization temperature/°C)	B (activation temperature/°C)	C (KOH/carbonized material ratio)	D (activation time/h)
1	300	600	1	0.5
2	350	650	2	1
3	400	700	3	1.5

a comparison with raw *C. oleifera* shell surface before the treatment. FT-IR analysis was applied to determine the functional groups present on the surface of *C. oleifera* shell activated carbon before and after adsorption by using FT-IR spectroscopy (Thermo Scientific Nicolet iS50, USA) with a potassium bromide pellet. The spectra were recorded from 4,000 to 500  $\text{cm}^{-1}$ . BET specific surface area and pore size were measured by using an automatic surface analyzer (Quantachrome Autosorb-iQ, USA).

### 2.5. Adsorption experiments

A mass of activated carbon was added to 100 mL of Cr(VI) solutions with the desired concentration in a 250 mL conical flask. These suspensions were adjusted to required pH value with 0.1 N HCl or NaOH, and then shaken in an air bath constant temperature oscillator (model THZ-C, Taicang Huamei Instrument Co., Ltd., Suzhou, JiangSu, China) at 175 rpm and constant temperatures. A small amount of solutions marked as samples were withdrawn at various time intervals and centrifuged at 9,000 rpm for 5 min. The absorbances of samples were measured using the spectrophotometer until the equilibriums were achieved. The adsorption capacity, ( $Q_t$ , mg/g), was determined as being the difference between the initial dichromate concentration ( $C_0$ , mg/L) and the concentration at a specific time ( $t$ ) or at equilibrium ( $C_e$ , mg/L), per gram of solid adsorbent, as outlined by Eq. (1):

$$Q_t = (C_0 - C_t) \times \frac{V}{m} \quad (1)$$

where  $m$  is the mass of adsorbent (g); and  $V$  is the volume of solution. The removal percentage ( $R\%$ ) of Cr(VI) was calculated using Eq. (2):

$$R(\%) = \frac{(C_0 - C_t)}{C_0} \times 100\% \quad (2)$$

### 2.6. Adsorption kinetics experiments

Adsorption kinetics analysis of Cr(VI) onto activated carbon were performed in each conical flask. A known amount of activated carbon (0.10 g) was placed inside the flask and 100 mL of solution with 500 mg/L of Cr(VI) at pH 1 was poured into the flask. The mixtures were then oscillated in 175 rpm at 25°C, 30°C, 35°C, and 45°C. The aliquots were removed and centrifuged for analysis at established time intervals.

### 2.7. Isotherm experiments

Equilibrium adsorption isotherms were obtained by exposing 100 mL of different initial concentrations of Cr(VI) (350, 400, 450, 500, 550, 600, and 700 mg/L), with 0.1 g activated carbon powders, respectively, until equilibrium was attained. Four different temperatures (25°C, 30°C, 35°C, and 45°C) were investigated and the individual adsorption isotherm curves at 25°C, 30°C, 35°C, and 45°C were obtained by plotting  $q_t$  vs.  $C_e$ .

## 3. Results and discussion

### 3.1. Thermogravimetry–derivative thermogravimetry

Thermo-gravimetric analysis of the powder crushed by *C. oleifera* shell (raw powder) was performed to study the process of carbonization as shown in Fig. 1. As can be seen from Fig. 1, there were three phases in whole pyrolysis process. 35°C–210°C was the first phase. The water including absorbed water, free water, and bound water was removed from the powder in this phase. In the second stage, sharp weight loss of the raw powder occurred at 210°C–500°C and the loss ratio was up to 54.2%. The raw powder experienced the thermal decomposition and carbonization during the phase. The derivative thermogravimetry (DTG) peaks at 292°C correspond to the decomposition of hemicelluloses, cellulose. Above 370°C–397°C, the lignin began to decompose. The pyrolysis process has completed until 502°C. At 502°C–900°C as the third phase, the weight loss curve became smooth and slightly. The carbon residue decreases to 43.9% at 500°C and 42.3% at 900°C. The residues mainly include fixed carbon and ash. It could be concluded from the analysis that the pyrolysis process of macromolecular organic components has completed at around 372°C. Finally, the range of carbonization temperature was set from 300°C to 400°C increased 50°C at a time.

### 3.2. Orthogonal experimental analysis

The orthogonal experiment analysis on the producing activated carbon from *C. oleifera* shell is shown in Table 2. The orthogonal experiment analysis indicates that the mass ratio of KOH to carbonized material and activation time affects the primary factor on the adsorption capacity of Cr(VI), but activation temperature and carbonization temperature were the secondary factors. The optimal condition is A3B2C3D2. Under the optimal condition, three times of parallel experiments were carried out and the results showed that the equilibrium adsorption capacity of Cr(VI) could reach 374.77, 368.45, and 370.16 mg/g. The experimental data are close to each other and better than the data listed in the orthogonal experiment. It indicates that the range

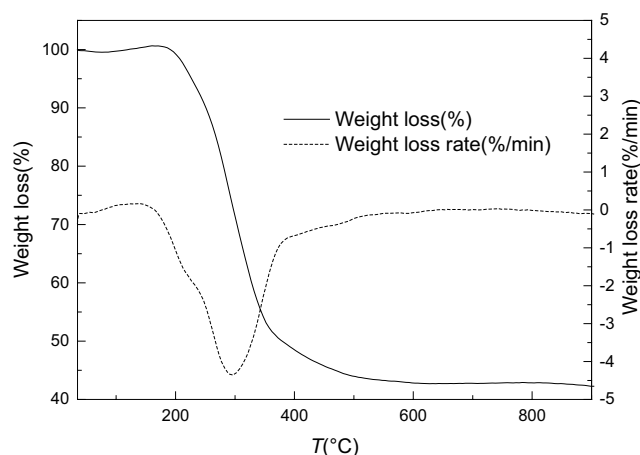


Fig. 1. TG-DTG of raw *Camellia oleifera* shell.

analysis is reliable. Therefore, the *C. oleifera* shell activated carbon would be prepared by the optimum conditions: carbonization temperature 400°C, activation temperature 650°C, KOH/carbonized material ratio 3, activation time 1 h, respectively, which was chosen as the suitable adsorbent for adsorbing Cr(VI) throughout all the remaining adsorption experiments.

### 3.3. Characterization of the activated carbon

#### 3.3.1. Scanning electron microscopy

The SEM results of the precursor and the activated carbon samples are shown in Fig. 2. Significant difference of surface morphology between the precursor (Fig. 2a) and the activated carbon (Fig. 2b) was vividly demonstrated. The precursor showed smooth and less porosity, while

after carbonization and activation, the activated carbon surfaces were irregular and rough with lots of newly formed pores and cavities. It indicates that the activated carbons prepared through carbonization and activated by potassium hydroxide have a higher degree of pore development than the precursor as can be seen from Fig. 2b. The result indicates that *C. oleifera* shell activated carbon which has a higher surface area and pore volume may be a more effective adsorbent compared to the raw *C. oleifera* shell.

#### 3.3.2. Nitrogen adsorption–desorption

N<sub>2</sub> adsorption–desorption isotherms and the pore size distribution of the activated carbon were presented in Figs. 3 and 4, with adsorption data obtained over a relative pressure ( $P/P_0$ ) range from 0.05 to 0.99 [26]. The average pore diameter was calculated to be 3.930 nm by

Table 2  
Results of orthogonal experiment and analysis

Experiment number	A	B	C	D	Q <sub>e</sub> (mg/g)
1	300	600	1	0.5	287.14
2	300	650	2	1.0	300.62
3	300	700	3	1.5	304.88
4	350	600	2	1.5	232.51
5	350	650	3	0.5	327.23
6	350	700	1	1.0	308.07
7	400	600	3	1.0	355.00
8	400	650	1	1.5	279.69
9	400	700	2	0.5	259.47
K1	297.55	291.55	291.63	291.28	
K2	289.27	302.51	264.20	321.23	
K3	298.05	290.81	329.04	272.36	
R	8.78	11.71	64.84	48.87	
Optimal condition	A3	B2	C3	D2	

\*A, carbonization temperature/°C; B, activation temperature/°C; C, the mass ratio of KOH to carbonized material; and D, activation time/h.

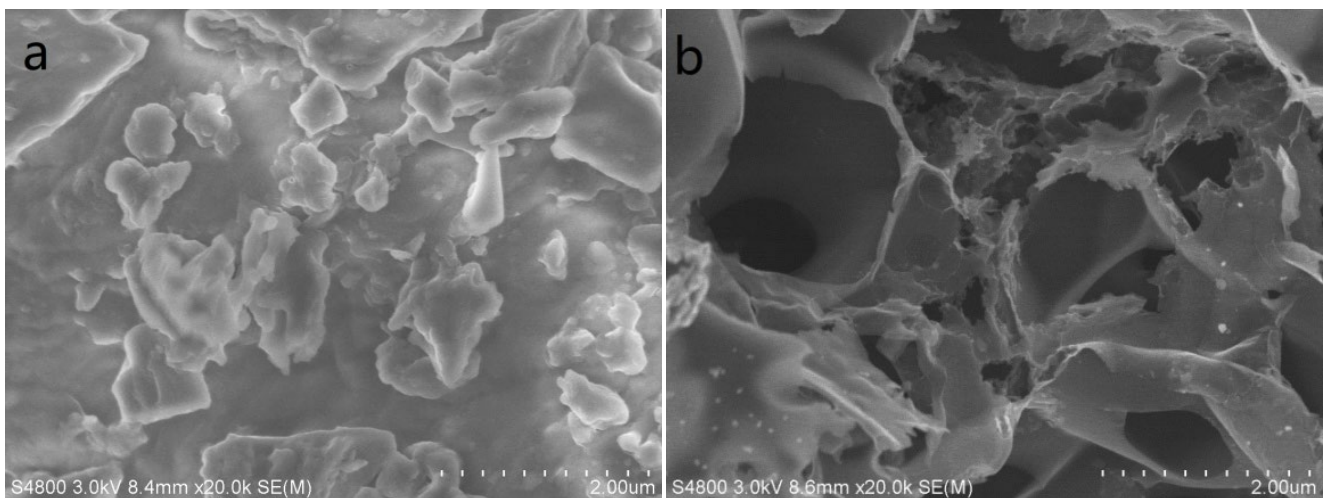


Fig. 2. SEM images of (a) raw *Camellia oleifera* shell and (b) *Camellia oleifera* shell activated carbon.

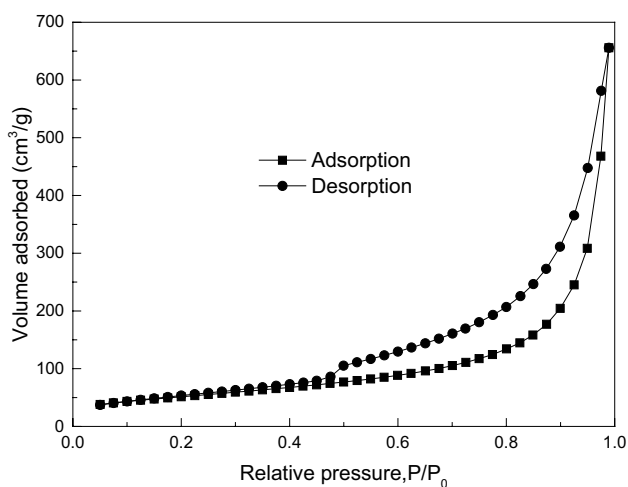


Fig. 3.  $N_2$  adsorption-desorption isotherm of the activated carbon.

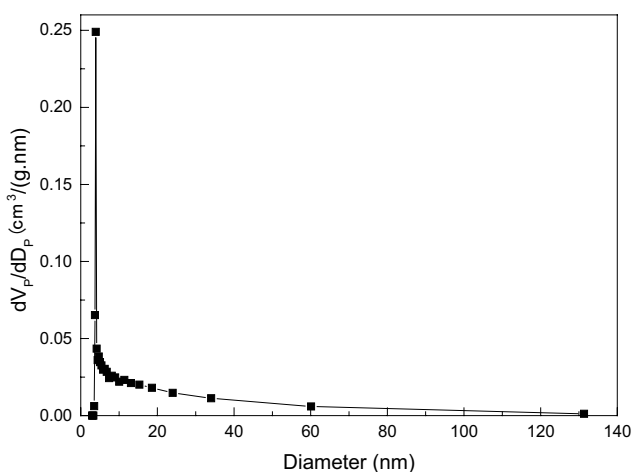


Fig. 4. Mesopore size distribution of activated carbon.

the Barrett-Joyner-Halenda (BJH) model, with the pore size distribution concentrating in the mesoporous range (2–50 nm). The BET surface area, pore volume and average pore diameter were determined to be 1,585.60  $m^2/g$ , 1.055  $cm^3/g$ , and 3.930 nm, respectively. The BET results indicate that activated carbon has a high potential as an efficient adsorbent.

### 3.3.3. FT-IR spectra analysis

The FT-IR spectra of raw material and activated carbon are shown in Fig. 5. The characteristic absorption bands at around 3,430  $cm^{-1}$  in raw material indicated the presence of O–H group stretching vibrations due to the cellulose, hemicelluloses, and lignin contained in the raw material. The broad peak at 2,920  $cm^{-1}$  was associated with C–H stretching vibrations which could be related to methyl, methylene, and methoxy groups. Bands at 1,732  $cm^{-1}$  confirmed the presence of carboxylic or ester groups. The band

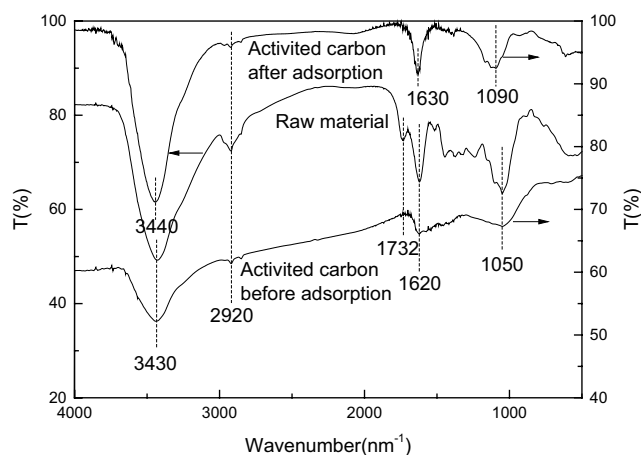


Fig. 5. FT-IR spectra of raw material, activated carbon before and after adsorption.

observed at 1,620  $cm^{-1}$  was associated with the C=C stretching vibration of the lignin aromatic ring or C=O stretching vibration of carboxylic groups. The peak at 1,050  $cm^{-1}$  should be attributed to the –OH stretching vibration [25]. The FT-IR spectra of activated carbon show that parts of the bands decreased even disappeared at the wavenumbers of 3,430; 2,920; 1,732; 1,620; and 1,050  $cm^{-1}$ . It indicated that the organics in the raw material such as cellulose, hemicelluloses, and lignin were decomposed between carbonization and activated process [27].

### 3.4. Effect of pH on adsorption

Solution pH was found to be an important controlling parameter in Cr(VI) adsorption processes. The effects of initial pH of solution on Cr(VI) adsorption are presented in Fig. 6. As seen in Fig. 6, the equilibrium adsorption capacity of Cr(VI) decreased from 385.30 to 297.37  $mg/g$ , when pH value increased from 2.0 to 7.0, showing that lower pH conditions of 2.0–5.0 are favorable for Cr(VI) removal using the investigated biochar. Based on the findings of FT-IR analysis, it was established that the surface of *C. oleifera* shell activated carbon contains carboxylic and phenolic hydroxyl groups. The pH dependence of Cr(VI) adsorption may be due to changes in the ionic state of these oxygen-containing functional groups, as well as Cr(VI) speciation [24,28]. As for the Cr(VI), the dominant species of Cr(VI) is  $HCrO_4^-$  at lower pH, and when the pH increases,  $HCrO_4^-$  is converted to  $CrO_4^{2-}$  and  $Cr_2O_7^{2-}$  [29]. At pH conditions below 5, the biochar surface is positive charged with  $H^+$  ions, which benefits the electrostatic attraction between  $HCrO_4^-$  and the surface of biochar [25]. The biochar surface was negatively charged under higher pH conditions, which was not supportive to adsorption. Thus, the optimum pH value of the experiments in this research was set at around 2.0.

### 3.5. Effect of adsorbent dose

The adsorption of Cr(VI) on adsorbents was studied at different adsorbent doses and the result is shown in Fig. 7.

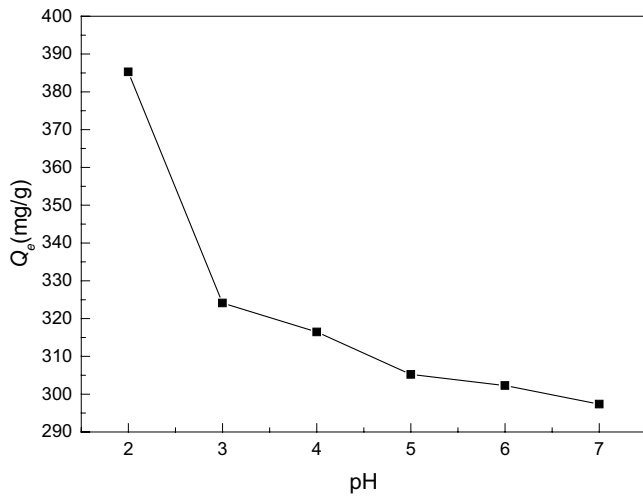


Fig. 6. Effect of pH on adsorption of Cr(VI).

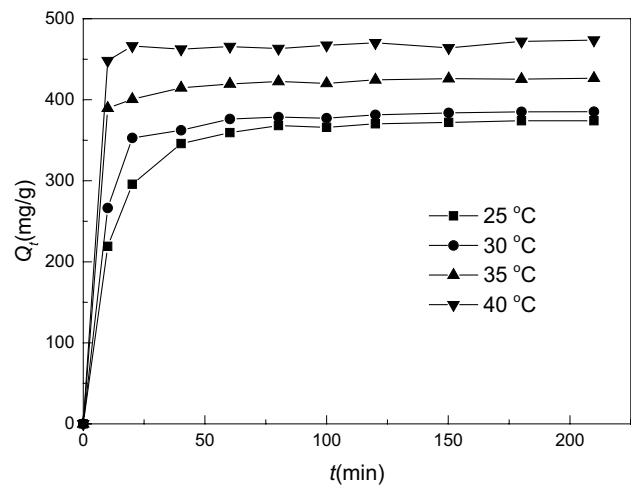


Fig. 8. Effect of adsorbent temperature and time on adsorption of Cr(VI).

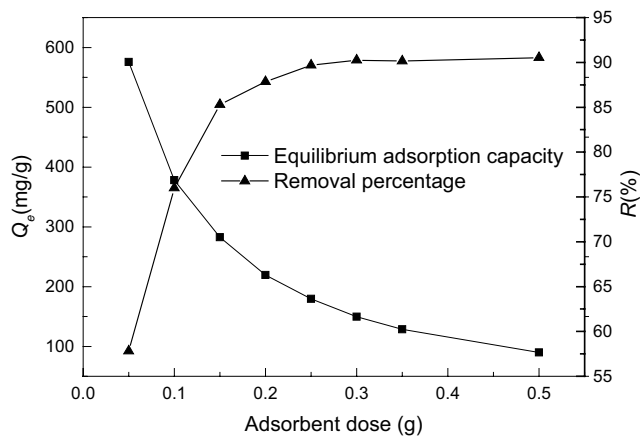


Fig. 7. Effect of adsorbent dose on adsorption of Cr(VI).

It can be clearly seen from Fig. 7 that with increase in the adsorbent dose, removal percentage of Cr(VI) is promoted. It may be due to the increase in adsorbent surface area and availability of more adsorption sites [30]. When the amount of the adsorbent reaches a certain value (more than 0.25 g), the removal percentage tends to be stabilized. Enough active sites have been provided that may lead to a stabilization of removal percentage. But unit adsorption is decreased with increase in adsorbent dose. This may be due to overlapping of adsorption sites as a result of overcrowding of adsorbent particles [31]. The excessive adsorbent dosing with the limited contaminant concentration in the solution that resulting in a large excess of active sites leads to a lower utility of sites. Therefore, the suitable adsorbent dosage was selected to be 0.25 g for Cr(VI) adsorption.

### 3.6. Effect of adsorption temperature and time

The effect of adsorption temperature and time were studied and the results are shown in Fig. 8. Fig. 8 indicates that the adsorption capacity is increased rapidly to the

maximum value in the first 10–40 min and then remained almost steady. The first step is rapid and can be attributed to the surface adsorption of contaminants onto the adsorbent surface; while the following step is slower and relates to the adsorption of contaminants onto the inner surfaces of the adsorbent [32]. It also could be seen from Fig. 8 that the adsorption capacity of Cr(VI) increases with the temperature rising from 25°C to 40°C, which indicates that the adsorption process of Cr(VI) is endothermic. Similar trends were also found with the biosorption of Cr(VI) onto longan seed activated carbon [2], apple peels activated carbon [33] and PEI modified P-doped oil-tea shell [34].

### 3.7. Adsorption kinetics

Adsorption mechanism depends on the transportation process as well as the physical and chemical properties of adsorbent, which is important information for designing batch adsorption systems [35,36]. In order to analyze the adsorption rate behavior of Cr(VI) on adsorbent at different temperatures, pseudo-first-order (Eq. (3)) and pseudo-second-order models (Eq. (4)) [37,38] was used to evaluate the adsorption kinetics.

$$\ln\left(1 - \frac{Q_t}{Q_e}\right) = -k_1 t \quad (3)$$

$$\frac{t}{Q_t} = \frac{1}{Q_e} t + \frac{1}{k_2 Q_e^2} \quad (4)$$

where  $Q_e$  (mg/g) is the amounts of adsorbate adsorbed at equilibrium.  $k_1$  (1/min) is the rate constant of pseudo first-order model.  $k_2$  (g/mg min) is the rate constant of pseudo-second-order model.

In order to examine conformity of both models and experimental results, the linear plots of  $\ln(1 - Q_t/Q_e) - t$  and  $(t/Q_t) - t$  were used for pseudo-first-order and pseudo-second-order kinetic models, respectively. The data are plotted and

shown in Fig. 9. The values of  $k_1$ ,  $k_2$ , and determination coefficient  $R^2$  obtained from the plots are given in Table 3.

As shown in Table 3, the small determination coefficients of the pseudo-first-order model indicate the poor correlation of Cr(VI) adsorption onto *C. oleifera* shell activated carbon. Application of the pseudo-second-order model provides much better determination coefficients. Furthermore, the determination coefficient values for the second-order kinetic model were higher than 0.9994. It is clear that Cr(VI) adsorption process follows the pseudo-second-order kinetic model. Therefore, it can be concluded that Cr(VI) adsorption onto the produced carbon consist of chemical adsorption due to the fact that the pseudo-second-order kinetic model suggests that the adsorption process involves chemisorptions mechanism.

The adsorption activation energy was calculated by the logarithmic form of the Arrhenius equation as follows.

$$\ln k_2 = \frac{-E_a}{RT} + \ln A \quad (5)$$

where  $T$  is the absolute temperature (K),  $R$  is the gas constant (8.314 J/mol K),  $E_a$  is the adsorption activation energy (kJ/mol), and  $A$  is frequency factor.

Pseudo-second-order rate constant was used as an adsorption rate constant. Activation energy was calculated from the linear plot of Arrhenius equation ( $R^2 = 0.9871$ ) as 99.070 kJ/mol. Weak van der Waals forces are responsible in

the case of physical adsorption and its activation energy is not more than 4.184 kJ/mol. 99.070 kJ/mol activation energy is high and can be an indicator of chemical adsorption or reduction reactions.

### 3.8. Adsorption isotherms

Adsorption isotherms are significant to design the adsorption processes, and they also provide adsorption capacity of the adsorbent under studied conditions. Although there are many adsorption isotherms models, Langmuir and Freundlich are the most frequently used equations in the literature, expressing the nonlinear relationship between adsorbed metal ion on the adsorbent and metal ion in the solution. These two-parameter models are simple and give a good description of experimental behavior in a large range of operating conditions [39]. Langmuir and Freundlich adsorption isotherm models were examined to describe adsorption equilibrium at different pH and temperature used in this study. The linear forms of these models were listed as follows [40].

$$\frac{C_e}{Q_e} = \frac{1}{Q_m} C_e + \frac{1}{Q_m K_L} \quad (6)$$

$$\lg Q_e = \frac{1}{n} \lg C_e + \lg K_F \quad (7)$$

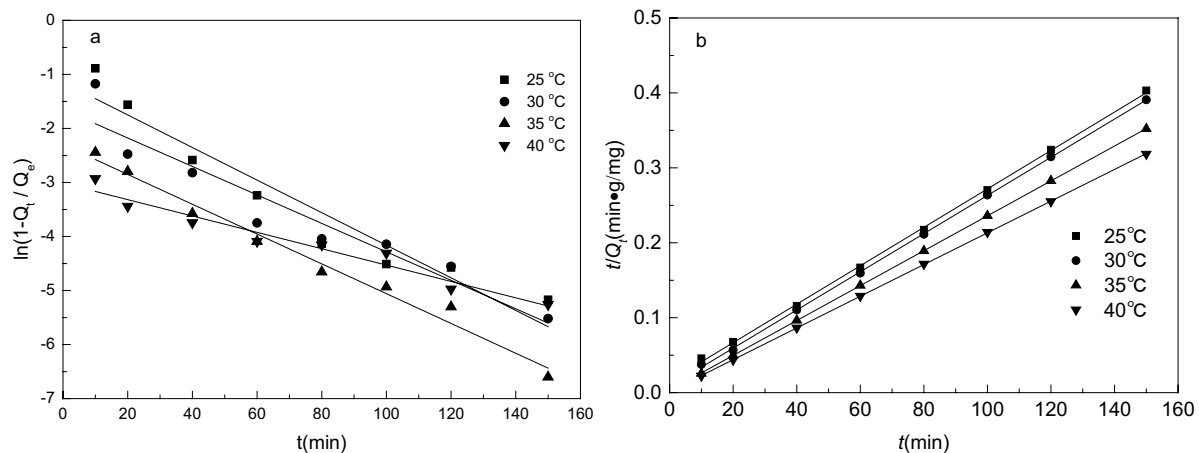


Fig. 9. Fitting curves by pseudo-first-order (a) and pseudo-second-order (b) kinetic models for adsorption.

Table 3  
Kinetics parameters for adsorption of Cr(VI)

$T$ (°C)	Pseudo-first-order kinetic model			Pseudo-second-order kinetic model		
	$Q_e$ (mg/g)	$k_1$ (min <sup>-1</sup> )	$R^2$	$k_2$ [g/(mg min)]	$R^2$	$Q_e$ (mg/g)
25	374.10	0.0302	0.9143	0.0004239	0.9994	390.63
30	385.30	0.0263	0.9011	0.0007723	0.9997	392.16
35	426.62	0.0276	0.9798	0.001774	0.9999	429.18
40	473.55	0.0151	0.9459	0.002691	0.9999	471.70

where  $Q_m$  (mg/g) is the mono layer adsorption capacity of the adsorbent.  $K_L$  is the Langmuir adsorption constant.  $K_F$  and  $n$  are the Freundlich constants, where  $K_F$  and  $n$  represent the adsorption capacity and intensity of adsorption, respectively. The Langmuir and Freundlich adsorption isotherms are displayed in Fig. 10. The values of the Langmuir constants, Freundlich constants, and the correlation coefficients are listed in Table 4.

As shown in Table 4, the determination coefficients ( $R^2$ ) of Langmuir model are all beyond 0.9676, which are higher than of Freundlich model at the three different temperatures, respectively. Therefore, it is clear that Langmuir model fits better to the experimental data than Freundlich model. It suggests that the adsorption of Cr(VI) is dominated by the mono-layer surface adsorption, and the similar results was found by Yang and Han [41].

For the removal of Cr(VI), *C. oleifera* shell activated carbon displays a high removal capacity (374.10 mg/g).

The results show better performance than many reported biomass-derived carbons listed in Table 5 [2]. This suggests that high quality activated carbon could be prepared by *C. oleifera* seed shell and be suitable for practical application.

Furthermore, the thermodynamic parameters of Cr(VI) adsorption, such as enthalpy change  $\Delta H^\circ$ , entropy change  $\Delta S^\circ$ , and Gibbs free energy change  $\Delta G^\circ$ , were calculated from the experimental results got at different temperatures using the following equations [42]:

$$\ln K_L = -\frac{\Delta H}{RT} + \frac{\Delta S}{R} \tag{8}$$

$$\Delta G = \Delta H - T\Delta S \tag{9}$$

The thermodynamic values of  $\Delta H^\circ$ ,  $\Delta S^\circ$ , and  $\Delta G^\circ$  were determined and are listed in Table 6. As shown in Table 6,

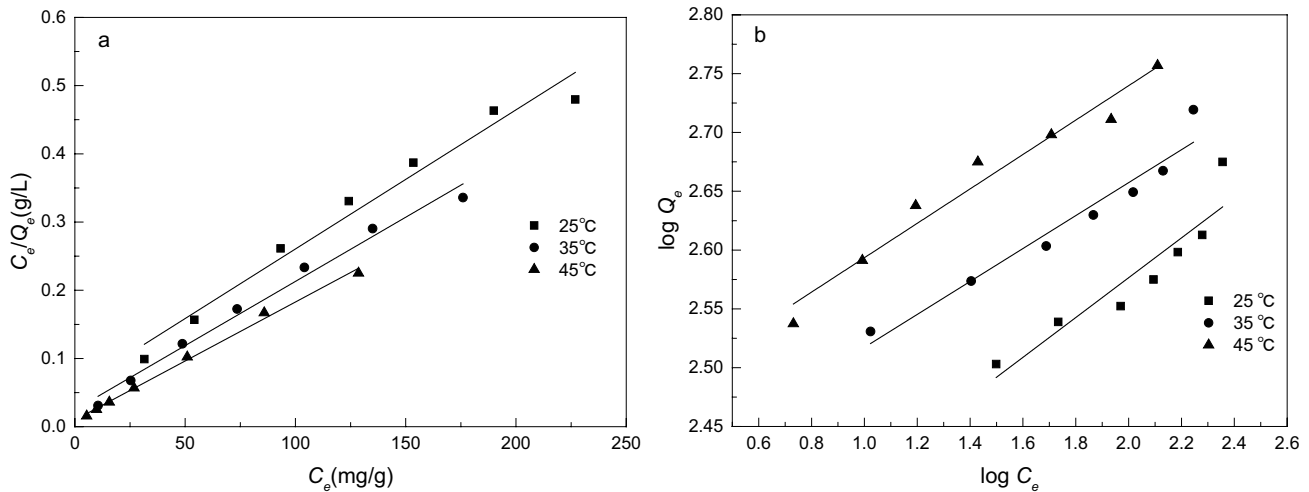


Fig. 10. Langmuir (a) and Freundlich (b) isotherm adsorption curves.

Table 4  
Correlated parameters of isotherm adsorption model

T (°C)	Langmuir model			Freundlich model		
	$K_L$ (L/mg)	$Q_m$ (mg/g)	$R^2$	$K_F$	$n^{-1}$	$R^2$
25	0.03606	490.20	0.9676	172.98	0.1693	0.9079
35	0.07581	531.91	0.9842	238.34	0.1401	0.9543
45	0.17528	578.03	0.9950	280.03	0.1463	0.9770

Table 5  
Maximum adsorption capacities ( $q_{max}$ ) of Cr(VI) for different biosorbents

Adsorbents	pH	Concentration (mg/L)	$q_{max}$ (mg/g)	References
Longan seed activated carbon	3	100	35.0	[2]
Apple peels activated carbon	2	50	36.0	[33]
PEI modified P-doped oil-tea shell	1	600	355.0	[34]
Ni/Al at PAB	2	250	271.5	[42]
<i>Camellia oleifera</i> shell activated carbon	2	500	374.1	Our work

Table 6  
Thermodynamic parameters for the adsorption of Cr(VI)

T (°C)	$\Delta H^\circ$ (kJ/mol)	$\Delta S^\circ$ (J/mol·K)	$\Delta G^\circ$ (kJ/mol)
25			-8.83
35	62.29	238.53	-11.22
45			-13.60

the negative  $\Delta G^\circ$  decreases slightly with the increasing temperature, which indicates that it is spontaneous in the process of the Cr(VI) adsorption on the activated carbon. The values of  $\Delta S^\circ$  are positive which signifies that the process of Cr(VI) adsorption on activated carbon is entropy-driven rather than enthalpy driven [43]. Moreover, the positive value of  $\Delta H^\circ$  confirmed the endothermic nature of the adsorption process and increasing temperature favors the adsorption as referred to in 3.6.

### 3.9. Proposed Cr(VI) removal mechanism

The possible adsorption mechanism of Cr(VI) was systematic investigated. The FT-IR of *C. oleifera* shell activated carbon before and after adsorption is shown in Fig. 5. Comparison of FT-IR spectra of *C. oleifera* shell activated carbon before adsorption (Fig. 5) led to the conclusion that the spectra were similar in their whole, however, with changes in intensity and shifts of some bands [32]. The peak around  $3,430\text{ cm}^{-1}$  was observed to shift to  $3,440\text{ cm}^{-1}$  after adsorption that corresponds to the O–H stretching. The C=C stretching vibration of the lignin aromatic ring or C=O stretching gives a peak at  $1,620\text{ cm}^{-1}$  which is shifted to  $1,630\text{ cm}^{-1}$  after fixation of Cr(VI). The peak at  $1,050\text{ cm}^{-1}$  in the *C. oleifera* shell activated carbon spectrum before Cr(VI) adsorption, which is due to the –OH stretching, is moved to  $1,090\text{ cm}^{-1}$  after adsorption. The functional groups which have been shifted after adsorption of Cr(VI) are involved in the adsorption of this latter. Herein, these observations could be concluded that O–H, C=C, C=O, –OH groups are involved in the binding of Cr(VI) with *C. oleifera* shell activated carbon.

To sum up, the adsorption mechanisms of Cr(VI) on *C. oleifera* shell activated carbon might be synergistic effects as follows [26,34]: (1) the electrostatic attraction, according to the pH effect on Cr(VI) adsorption; (2) reduction and precipitation, considering the significant difference of FT-IR spectra analysis on before and after adsorption; (3) physical adsorption on the basis of porous structures of *C. oleifera* shell activated carbon.

## 4. Conclusions

- Through the TG-DTG analysis, the range of carbonization temperature was set from  $300^\circ\text{C}$  to  $400^\circ\text{C}$  increased  $50^\circ\text{C}$  at a time.
- The activated carbon could be synthesized from *C. oleifera* shell with potassium hydroxide. According to the orthogonal experiment, the results show that the optimum carbonization conditions are as follows: carbonization temperature of  $350^\circ\text{C}$ , activation temperature of  $600^\circ\text{C}$ , KOH/carbonized material ratio of 3, and activation time

of 1 h, respectively. The surface of the activated carbon has a higher surface area and pore volume than the raw material shown by SEM images.

- The batch experiments indicate that the optimum pH value is 2, the suitable adsorbent dosage is 0.25 g, and the adsorption capacity increases with the rising of temperature. The adsorption process follows the pseudo-second-order kinetic model and fits better to the Langmuir model. The process of Cr(VI) adsorption on activated carbon is entropy-driven and endothermic.
- All the findings demonstrate that biochar prepared by *C. oleifera* shell with KOH activation can be an effective and efficient adsorbent for Cr(VI) adsorption in aqueous solution.

## Acknowledgments

We acknowledge the financial support for this work from the Natural Science Foundation of Fujian Province (No. 2019J05127), the Educational Research Project of Young and Middle-aged Teacher of Fujian Province (Nos. JT180625, JT180333 and JAT190406), the Fujian Province Innovation and Entrepreneurship Talents (S201910388075), the Central Government Guides Local Science and Technology Development Project (2019L3013), the China Scholarship Council (No. 201908350057).

## References

- [1] J. Khabibi, W. Syafii, R.K. Sari, Reducing hazardous heavy metal ions using mangium bark waste, *Environ. Sci. Pollut. Res. Int.*, 23 (2016) 16631–16640.
- [2] J. Yang, M. Yu, W. Chen, Adsorption of hexavalent chromium from aqueous solution by activated carbon prepared from longan seed: kinetics, equilibrium and thermodynamics, *J. Ind. Eng. Chem.*, 21 (2015) 414–422.
- [3] J. Zhang, P. Zheng, A preliminary investigation of the mechanism of hexavalent chromium removal by corn-bran residue and derived chars, *RSC Adv.*, 5 (2015) 17768–17774.
- [4] S. Srivastava, S.B. Agrawal, M.K. Mondal, Biosorption isotherms and kinetics on removal of Cr(VI) using native and chemically modified *Lagerstroemia speciosa* bark, *Ecol. Eng.*, 85 (2015) 56–66.
- [5] A. Idris, N. Hassan, N.S.M. Ismail, E. Misran, N.M. Yusof, A.-F. Ngomsik, A. Bee, Photocatalytic magnetic separable beads for chromium(VI) reduction, *Water Res.*, 44 (2010) 1683–1688.
- [6] B. Neppolian, P. Karthik, H. Yamashita, T. Kamegawa, M. Wen, Synthesis of highly visible light active  $\text{TiO}_2$ -2-naphthol surface complex and its application in photocatalytic chromium(VI) reduction, *RSC Adv.*, 5 (2015) 39752–39759.
- [7] L. Liu, Y. Xu, K. Wang, K. Li, L. Xu, J. Wang, J. Wang, Fabrication of a novel conductive ultrafiltration membrane and its application for electrochemical removal of hexavalent chromium, *J. Membr. Sci.*, 584 (2019) 191–201.
- [8] X.Z. Wei, Z.Q. Gan, Y.J. Shen, Z.L. Qiu, L.F. Fang, B.K. Zhu, Negatively-charged nanofiltration membrane and its hexavalent chromium removal performance, *J. Colloid Interface Sci.*, 553 (2019) 475–483.
- [9] Z. Chen, B. Wei, S. Yang, Q. Li, L. Liu, S. Yu, T. Wen, B. Hu, J. Chen, X. Wang, Synthesis of PANI/AlOOH composite for Cr(VI) adsorption and reduction from aqueous solutions, *ChemistrySelect*, 4 (2019) 2352–2362.
- [10] S. Sessarego, S.C.G. Rodrigues, Y. Xiao, Q. Lu, J.M. Hill, Phosphonium-enhanced chitosan for Cr(VI) adsorption in wastewater treatment, *Carbohydr. Polym.*, 211 (2019) 249–256.
- [11] S. Hassanpour, M. Taghizadeh, Y. Yamini, Magnetic Cr(VI) ion imprinted polymer for the fast selective adsorption of Cr(VI) from aqueous solution, *J. Polym. Environ.*, 26 (2017) 101–115.

- [12] S. Patnaik, D.P. Sahoo, K.M. Parida, Bimetallic co-effect of Au-Pd alloyed nanoparticles on mesoporous silica modified g-C<sub>3</sub>N<sub>4</sub> for single and simultaneous photocatalytic oxidation of phenol and reduction of hexavalent chromium, *J. Colloid Interface Sci.*, 560 (2019) 519–535.
- [13] L. Tang, Y. Fang, Y. Pang, G. Zeng, J. Wang, Y. Zhou, Y. Deng, G. Yang, Y. Cai, J. Chen, Synergistic adsorption and reduction of hexavalent chromium using highly uniform polyaniline-magnetic mesoporous silica composite, *Chem. Eng. J.*, 254 (2014) 302–312.
- [14] B. Qiu, C. Xu, D. Sun, H. Yi, J. Guo, X. Zhang, H. Qu, M. Guerrero, X. Wang, N. Noel, Z. Luo, Z. Guo, S. Wei, Polyaniline coated ethyl cellulose with improved hexavalent chromium removal, *ACS Sustainable Chem. Eng.*, 2 (2014) 2070–2080.
- [15] Z. Zheng, J. Yang, J. Guo, Preparation of graphene and its adsorption to Cr(VI), *Chin. J. Process Eng.*, 17 (2017) 1085–1090.
- [16] C. Zheng, H. Zheng, Y. Sun, B. Xu, Y. Wang, X. Zheng, Y. Wang, Simultaneous adsorption and reduction of hexavalent chromium on the poly(4-vinyl pyridine) decorated magnetic chitosan biopolymer in aqueous solution, *Bioresour. Technol.*, 293 (2019) 122038.
- [17] K. Selvi, S. Pattabhi, K. Kadirvelu, Removal of Cr(VI) from aqueous solution by adsorption onto activated carbon, *Bioresour. Technol.*, 80 (2001) 87–89.
- [18] C.G. Joseph, S.M. Anisuzzaman, W.M.A.W. Daud, D. Krishnaih, K.A. Ng, Chlorinated phenol removal from aqueous media by tea (*Camellia sinensis*) leaf waste tailored activated carbon, *IOP Conf. Ser.: Mater. Sci. Eng.*, 206 (2017) 012099, doi: 10.1088/1757-899X/206/1/012099.
- [19] K. Sartova, E. Omurzak, G. Kambarova, I. Dzhumaev, B. Borkoev, Z. Abdullaeva, Activated carbon obtained from the cotton processing wastes, *Diamond Relat. Mater.*, 91 (2019) 90–97.
- [20] Y. Huang, Y. Liu, G. Zhao, J.Y. Chen, Sustainable activated carbon fiber from sawdust by reactivation for high-performance supercapacitors, *J. Mater. Sci.*, 52 (2016) 478–488.
- [21] S. Kumagai, Y. Shimizu, Y. Toida, Y. Enda, Removal of dibenzothiophenes in kerosene by adsorption on rice husk activated carbon, *Fuel*, 88 (2009) 1975–1982.
- [22] H. Li, Y. Shuaishuai, S. HuiZhen, L. Xiaohui, Production of activated carbon from cow manure for wastewater treatment, *Bioresources*, 13 (2018) 3135–3143.
- [23] H. Demiral, C. Güngör, Adsorption of copper(II) from aqueous solutions on activated carbon prepared from grape bagasse, *J. Cleaner Prod.*, 124 (2016) 103–113.
- [24] H. Guo, C. Bi, C. Zeng, W. Ma, L. Yan, K. Li, K. Wei, *Camellia oleifera* seed shell carbon as an efficient renewable bio-adsorbent for the adsorption removal of hexavalent chromium and methylene blue from aqueous solution, *J. Mol. Liq.*, 249 (2018) 629–636.
- [25] Y. Liu, X. Li, J. Zhou, W. He, Preparation and characterization of *Camellia oleifera* nut shell-based bioadsorbent and its application for heavy metals removal, *BioResources*, 14 (2019) 234–250.
- [26] J. Valentin-Reyes, R.B. Garcia-Reyes, A. Garcia-Gonzalez, E. Soto-Regalado, F. Cerino-Cordova, Adsorption mechanisms of hexavalent chromium from aqueous solutions on modified activated carbons, *J. Environ. Manage.*, 236 (2019) 815–822.
- [27] L.H. Velazquez-Jimenez, A. Pavlick, J.R. Rangel-Mendez, Chemical characterization of raw and treated agave bagasse and its potential as adsorbent of metal cations from water, *Ind. Crop. Prod.*, 43 (2013) 200–206.
- [28] U.K. Garg, M.P. Kaur, V.K. Garg, D. Sud, Removal of hexavalent chromium from aqueous solution by agricultural waste biomass, *J. Hazard. Mater.*, 140 (2007) 60–68.
- [29] A.H.M.G. Hyder, S.A. Begum, N.O. Egiebor, Adsorption isotherm and kinetic studies of hexavalent chromium removal from aqueous solution onto bone char, *J. Environ. Chem. Eng.*, 3 (2015) 1329–1336.
- [30] V. Garg, R. Gupta, R. Kumar, R. Gupta, Adsorption of chromium from aqueous solution on treated sawdust, *Bioresour. Technol.*, 92 (2004) 79–81.
- [31] C. Namasivayam, D. Prabha, M. Kumutha, Removal of direct red and acid brilliant blue by adsorption on to banana pith, *Bioresour. Technol.*, 64 (1998) 77–79.
- [32] M. Thirumavalavan, Y.-L. Lai, J.-F. Lee, Fourier transform infrared spectroscopic analysis of fruit peels before and after the adsorption of heavy metal ions from aqueous solution, *J. Chem. Eng. Data*, 56 (2011) 2249–2255.
- [33] I. Enniya, L. Rghioui, A. Jourani, Adsorption of hexavalent chromium in aqueous solution on activated carbon prepared from apple peels, *Sustainable Chem. Pharm.*, 7 (2018) 9–16.
- [34] S. Chen, J. Wang, Z. Wu, Q. Deng, W. Tu, G. Dai, Z. Zeng, S. Deng, Enhanced Cr(VI) removal by polyethylenimine- and phosphorus-codoped hierarchical porous carbons, *J. Colloid Interface Sci.*, 523 (2018) 110–120.
- [35] D. Duranoğlu, A.W. Trochimczuk, U. Beker, Kinetics and thermodynamics of hexavalent chromium adsorption onto activated carbon derived from acrylonitrile-divinylbenzene copolymer, *Chem. Eng. J.*, 187 (2012) 193–202.
- [36] P. Maneechakr, S. Karnjanakom, Adsorption behaviour of Fe(II) and Cr(VI) on activated carbon: surface chemistry, isotherm, kinetic and thermodynamic studies, *J. Chem. Thermodyn.*, 106 (2017) 104–112.
- [37] Z.A. Al-Othman, R. Ali, M. Naushad, Hexavalent chromium removal from aqueous medium by activated carbon prepared from peanut shell: adsorption kinetics, equilibrium and thermodynamic studies, *Chem. Eng. J.*, 184 (2012) 238–247.
- [38] Y. Wang, S. Huang, S. Shao, L. Qian, P. Xu, Studies on bioactivities of tea (*Camellia sinensis* L.) fruit peel extracts: antioxidant activity and inhibitory potential against  $\alpha$ -glucosidase and  $\alpha$ -amylase *in vitro*, *Ind. Crop. Prod.*, 37 (2012) 520–526.
- [39] Z. Aksu, E. Balibek, Chromium(VI) biosorption by dried *Rhizopus arrhizus*: effect of salt (NaCl) concentration on equilibrium and kinetic parameters, *J. Hazard. Mater.*, 145 (2007) 210–220.
- [40] L. Wang, W. Liu, T. Wang, J. Ni, Highly efficient adsorption of Cr(VI) from aqueous solutions by amino-functionalized titanate nanotubes, *Chem. Eng. J.*, 225 (2013) 153–163.
- [41] J. Yang, S. Han, Kinetics and equilibrium study for the adsorption of lysine on activated carbon derived from coconut shell, *Desal. Water Treat.*, 120 (2018) 261–271.
- [42] A.M. Aljeboree, A.N. Alshirifi, A.F. Alkaim, Kinetics and equilibrium study for the adsorption of textile dyes on coconut shell activated carbon, *Arabian J. Chem.*, 10 (2017) S3381–S3393.
- [43] S. Banerjee, Y.C. Sharma, Equilibrium and kinetic studies for removal of malachite green from aqueous solution by a low cost activated carbon, *J. Ind. Eng. Chem.*, 19 (2013) 1099–1105.